ACS OMEGA

http://pubs.acs.org/journal/acsodf

Article

Blending with Poly(L-lactic acid) Improves the Printability of Poly(L-lactide-*co*-caprolactone) and Enhances the Potential Application in Cartilage Tissue Engineering

Ruiping Duan, Yimeng Wang, Yiyun Zhang, Ziqiang Wang, Fuchong Du, Bo Du, Danning Su, Lingrong Liu, Xuemin Li,* and Qiqing Zhang*

Cite This: *ACS Omega* 2021, 6, 18300−18313

Read Online

ACCESS | Metrics & More | Article Recommendations | Supporting Information

ABSTRACT: Poly(L-lactide-*co*-caprolactone) (PLCL, 50:50) has been used in cartilage tissue engineering because of its high elasticity. However, its mechanical properties, including its rigidity and viscoelasticity, must be improved for compatibility with native cartilage. In this study, a set of PLCL/poly(L-lactic acid) (PLLA) blends was prepared by blending with different mass ratios of PLLA that range from 10 to 50%, using thermoplastic techniques. After testing the properties of these PLCL/PLLA blends, they were used to fabricate scaffolds by the 3D printing technology. The structures and viscoelastic behavior of the PLCL/PLLA scaffolds were determined, and then, the potential application of the scaffolds in cartilage tissue engineering was evaluated by chondrocytes culture. All blends demonstrate good thermal stability for the 3D printing technology. All blends show good toughness, while the rigidity of PLCL is increased through PLLA blending, and Young's modulus of blends with 10−20% PLLA is similar to that of native cartilage. Furthermore, blending with PLLA improves the processability of PLCL for 3D printing, and the compression modulus and viscoelasticity of 3D-printed PLCL/PLLA scaffolds are different from that of PLCL. Additionally, the stress relaxation time ($t_{1/2}$) of the PLCL/PLLA scaffolds, which is important for chondrogenesis, is dramatically shortened compared with the pure PLCL scaffold at the same 3D-printing filling rate. Consistently, the PLCL90PLLA10 scaffold at a 70% filling rate with much shorter $t_{1/2}$ is more conducive to the proliferation and chondrogenesis of *in vitro* seeded chondrocytes accompanied by upregulated expression of SOX9 than the PLCL scaffold. Taken together, these results demonstrate that blending with PLLA improves the printability of PLCL and enhances its potential application, particularly PLCL/PLLA scaffolds with a low ratio of PLLA, in cartilage tissue engineering.

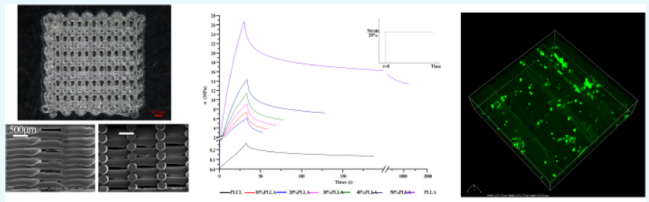

The morphology and mechanical properties of of the 3D-printed PLCL/PLLA scaffolds, and immunofluorescence staining of type II collagen of chondrocytes seeded on PLCL90PLLA10 scaffold.

1. INTRODUCTION

Aliphatic polyesters, such as poly(L-lactic acid) (PLLA), poly(e-caprolactone) (PCL), and poly(L-lactide-*co*-caprolactone) (PLCL) copolymers, have been widely applied in biomedicine.[1] These polymers exhibit excellent mechanical properties, biocompatibility, and biodegradability and can be manufactured into various implantable devices. In particular, with the development of three-dimensional (3D) printing technology, these polymers are promising candidates for the construction of complex-shaped scaffolds in tissue engineering.[2−5]

Among these aliphatic polyesters, PLCL has been widely applied in tissue engineering and tissue repair. PLCL is an amorphous copolymer composed of a soft segment of ε-caprolactone moieties and a hard segment containing L-lactide units.[6] It exhibits excellent mechanical properties as an elastomer and has a controlled degradation rate.[7] Compared with other synthetic biodegradable polymers, PLCL as a thermoplastic−elastomeric material presents good ductile behavior with a high elongation at break and a high elastic recovery capacity.[8−12] PLCL has been approved by the US FDA for clinical applications in vascular prostheses, peripheral nerve repair, and urethral reconstruction.[7−12] In particular, PLCL scaffolds exhibit mechanical properties of toughness similar to native cartilage. Therefore, PLCL is a promising candidate for the construction of mechano-stimulating tissue engineering scaffolds for cartilages.[13]

Various PLCL-based scaffolds have been developed for cartilage tissue engineering. Previously, because of their highly flexible and elastic properties, single PLCL scaffolds were directly fabricated using various approaches, such as salt impregnation, leaching, supercritical fluid processing, gel pressing, laser micromachining, and thermal crimping.[14−19] Subsequently, to improve mechanical properties and bio-

Received: April 26, 2021
Accepted: June 25, 2021
Published: July 8, 2021

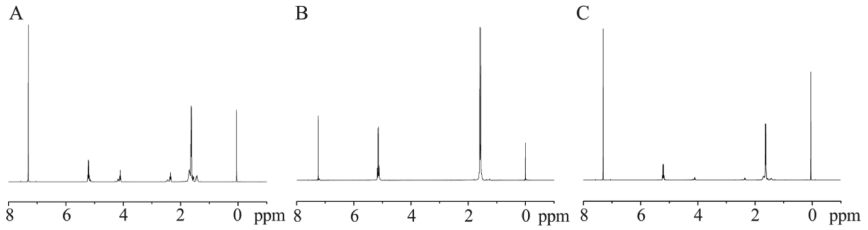

Figure 1. ^{1}H NMR spectra for (A) PLCL, (B) PLLA, and (C) PLCL50PLLA50.

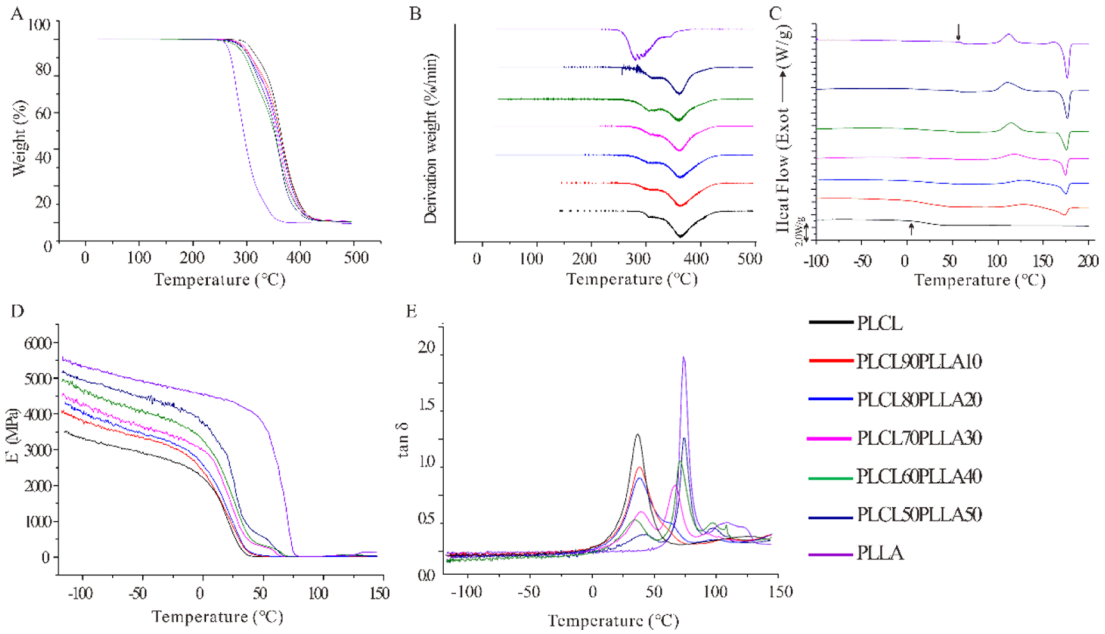

Figure 2. (A) TGA, (B) DTG, (C) DSC, and (D,E) DMA curves of PLCL/PLLA blends. The arrows in (C) indicate the T_g of PLCL and PLLA, respectively. (D) Storage modulus (E') and (E) loss factor (tan δ) of DMA.

activities, various modified PLCL scaffolds have been developed, such as PLCL/collagen, gelatin-incorporated PLCL, biphasic PLCL, fibrin and PLCL hybrid, chitosan-modified PLCL, peptide-modified PLCL, polymer microspheres, hydrogel-integrated PLCL, growth-factor-loaded PLCL, and 3D-printed PLCL-based biofunctionalized scaffolds.[13,20−27] These scaffolds are promising for applications in cartilage tissue engineering. However, the elastic modulus of most of these scaffolds is lower than that of native cartilage or the optimal elastic modulus for osteochondral repair.[18,28] In addition, the viscoelastic properties of most of these scaffolds are unclear but crucial in cartilage formation, repair, and regeneration.[29−32] Recently, it has been highlighted that the viscoelasticity, rather than the elasticity of the matrix, especially stress relaxation, is a key parameter in cartilage tissue engineering.[32−35] Therefore, the mechanical properties of PLCL-based tissue engineering scaffolds for cartilages must be improved; in particular, the rigidity and stress relaxation should mimic those of native tissues.

More recently, Ugartemendia *et al.* investigated the properties of a composite comprising PLLA and PLCL. They discovered that the toughness of PLLA was improved considerably by blending it with PLCL. More interestingly, their results demonstrated that the elastic modulus and tensile strength of blends with PLCL at ratios of 60 or 80% increase compared with that of pure PLCL.[36] These results indicate that PLLA can improve the mechanical properties of PLCL.

In this study, the potential application of PLCL/PLLA blends in cartilage tissue engineering was investigated. A set of PLCL/PLLA blends was prepared *via* thermoplastic technology using different mass ratios of PLCL and PLLA at first. Subsequently, the thermal, mechanical, and rheological properties as well as the structures of the blends were determined. Furthermore, scaffolds of these PLCL/PLLA blends were fabricated *via* melt-extrusion-based 3D printing due to both PLLA and PLCL can be 3D printed into a 3D porous structure.[5,37] Furthermore, the macro-/microstructures and mechanical properties of the scaffolds were determined. Finally, the potential application of these scaffolds in cartilage tissue engineering was evaluated by chondrocyte seeding, mRNA expression, and immunofluorescence staining of the extracellular matrix (ECM) of cartilage.

2. RESULTS AND DISCUSSION

2.1. Component Analysis of PLCL/PLLA Blends. To confirm the chemical composition of the blends, the composition was analyzed using NMR. Figure 1 shows the ^{1}H NMR spectra of PLCL, PLLA, and PLCL50PLLA50 blend (initial mass ratio of 50:50). The signals at δ 1.35−1.67 ppm, δ 2.3 ppm, and δ 4.03 ppm, as shown in Figure 1A, represent the peaks of $CH_2CH_2CH_2$, CH_2CO, and CH_2O of CL, respectively, whereas the signals at δ 1.55 and 5.2 ppm, as shown in Figure 1B, represent the peaks of CH_3 and CH of LA, respectively. As shown in Figure 1C, both the CL and LA

https://doi.org/10.1021/acsomega.1c02190
ACS Omega 2021, 6, 18300−18313

signals are present in the 1H NMR spectra of PLCL/PLLA blends, the lactic acid/co-caprolactone (LA/CL) molar ratio in the PLCL copolymers can be calculated using the integration ratio of peaks at 5.2 ppm for the LA unit and 4.03 ppm for the CL unit.[38] In this study, the initial molar composition of LA is nearly 77.5%, whereas that of CL is approximately 22.5% of the PLCL copolymer calculated by Figure 1A. The mass fraction of PLLA in the PLCL50PLLA50 blend (Figure 1C) is approximately 47.50% after calculating the molar ratio of LA/CL, which is slightly lower than the theoretical value. This decrease in the mass fraction of PLLA in the blend may be due to the small amount of thermal degradation of PLLA during the preparation through intramolecular transesterification.[39] In general, these results indicate that blending did not cause obvious chemical structural changes in PLCL and PLLA.

2.2. Thermal Stability and Behavior of PLCL/PLLA Blends. To evaluate the thermal stability of PLCL/PLLA blends for fused deposition modeling (FDM), they were tested using TGA.[40] Figure 2A,B shows the profiles from the TGA and the derivative thermogravimetry (DTG) of all samples. According to the TGA and DTG results, the decomposition temperatures were extracted (Table 1). Here, the temperature of 5 wt % weight loss of the blends is designated as the onset temperature of thermal decomposition (T_{onset}), which is an important indicator for measuring the heat resistance of the material. The temperature of the maximum thermal weight loss rate is designated as the maximum decomposition rate temperature (T_{max}). The T_{onset} decreases from 307.9 °C (PLCL) to approximately 295 °C (blends), whereas their T_{max} shows no obvious changes. Interestingly, all the PLCL/PLLA blends show two T_{max} values, as shown by neat PLCL. Furthermore, it can be observed that the maximum weight loss rate ($R_{max}1$) increases with PLLA rather than with pure PLCL, whereas $T_{max}1$ increases only slightly. Therefore, the $T_{max}1$ of PLCL can be attributed to the relatively low decomposition temperature of LA, whereas the relatively constant $T_{max}2$ is the decomposition temperature of CL. Meanwhile, for all blends and the neat PLCL, both T_{onset} and $T_{max}1$ are higher than those of neat PLLA, which suggests that CL might confer a protective action on LA.[41] In general, all the PLCL/PLLA blends demonstrate good thermal stability, and the temperatures of their decomposition are high to about ∼300 °C.

Table 1. Summary of the TGA Results of PLCL/PLLA Blends[a]

		T_{max}/°C		R_{max}/wt %	
sample	T_{onset}/°C	1	2	1	2
PLCL	307.9	304.6	363.2	3.6	49.5
PLCL90PLLA10	296.4	305.1	363.6	8.3	53.3
PLCL80PLLA20	293.5	305.7	362.4	10.5	54.7
PLCL70PLLA30	297.4	307.2	362.2	10.1	59.3
PLCL60PLLA40	296.3	306.9	360.2	15.9	62.1
PLCL50PLLA50	293.3	309.6	360.4	13.1	62.0
PLLA	265.6	281.7	–	28.4	–

[a]Note: T_{onset}, the onset temperature of thermal degradation; T_{max}, the temperature of maximum thermal weight loss rate; and R_{max}, the maximum weight loss rate.

Furthermore, the thermal properties of the blends were determined by differential scanning calorimetry (DSC) (Figure 2C). Table 2 shows the values of thermal properties of the samples obtained from the DSC curves. The result of PLCL only shows one glass-transition temperature (T_g) at approximately 15 °C without the crystallization temperature (T_c) and melting temperature (T_m), which is consistent with the properties of the amorphous copolymer. However, it is clear that PLLA shows a single T_g at approximately 59.6 °C. Interestingly, only a single T_g is distinguishable from the PLCL90PLLA10 blend at 16.5 °C, indicating that this blend is completely miscible.[36] In contrast, two T_g values, T_g1 and T_g2, of the blends at 20−50% mass ratio of PLLA can be seen, which can be ascribed to PLCL and PLLA, respectively, indicating these blends are partially miscible.[36,42] As shown in Figure 2C, a distinct "cold crystallization" of PLLA occurs at approximately 112 °C, and no crystal peak is observed for pure PLCL, whereas crystallization peaks appear in all PLCL/PLLA blends. The T_c of all PLCL/PLLA blends differed from that of pure PLLA (Table 2). In particular, the T_c of the PLCL90PLLA10 blend is the highest (nearly 128.3 °C); subsequently, the T_c decreases with increasing PLLA and gradually approaches that of pure PLLA. In contrast, the enthalpy of cold crystallization (ΔH_c) and the melting enthalpy (ΔH_m) of the blends increase with the amount of PLLA. Together, these results indicate that after blending, PLCL retains its amorphous form, whereas PLLA demonstrates the crystallizability.[36,41] However, the values of $\Delta H_m - \Delta H_c$ are constant around 7−10 J/g among all blends, indicating that the crystallinity in blends do not vary substantially. This finding is confirmed by the results of X-ray diffraction (XRD) (Figure S2). The XRD spectra of PLCL and blends exhibit two main diffraction peaks at 2θ angles of 17.0 and 19.4° approximately, suggesting that the changes of the crystallinity in blends are not significant after PLLA addition. The T_m of the blends are increased from 172.9 to 176.4 °C with the increase of the ratios of PLLA, which are significantly lower than the temperatures of decomposition of them. On the other hand, this result indicates that the hot processing temperature of the blends should be higher than the T_m of them, and it was 185 °C for extrusion and FDM in our current study.

Table 2. Thermal Properties of PLCL/PLLA Blends

sample	T_g1/°C	T_g2/°C	T_c/°C	ΔH_c/J·g^{-1}	T_m/°C	ΔH_m/J·g^{-1}
PLCL	15.2	–	–	–	–	–
PLCL90PLLA10	16.5	–	128.3	15.0	172.9	26.8
PLCL80PLLA20	15.6	48.9	127.9	38.9	174.7	45.1
PLCL70PLLA30	15.3	52.1	118.2	43.5	174.4	53.2
PLCL60PLLA40	16.8	51.1	114.3	52.8	175.4	58.4
PLCL50PLLA50	18.8	55.6	110.3	59.0	176.4	66.2
PLLA	–	59.6	112.0	55.4	176.3	62.7

https://doi.org/10.1021/acsomega.1c02190
ACS Omega 2021, 6, 18300−18313

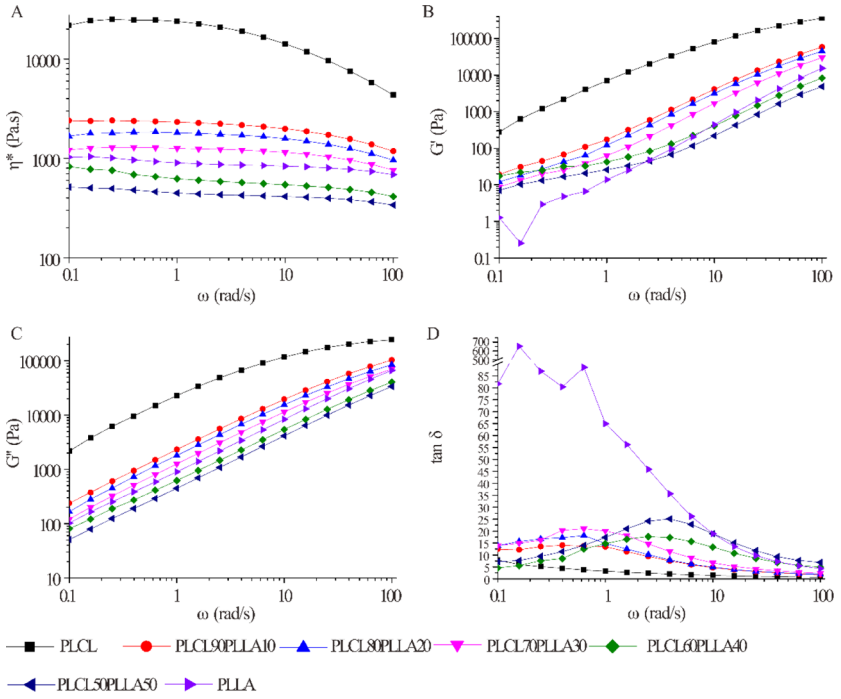

Figure 3. Rheological properties of PLCL/PLLA blends as a function of angular frequency at 185 °C. (A) Complex viscosity; (B) storage modulus; (C) loss modulus; and (D) loss tangent.

Figure 2D shows the curves of the storage modulus (E') of the blends as a function of temperature after dynamic thermomechanical analysis (DMA) tests. It is apparent that the E' values of all the PLCL/PLLA blends are higher than that of pure PLCL. PLLA is a polymer that displays generally high modulus, and blending it to PLCL can increase the overall rigidity of the blends.[36] Also, the inter- and intramolecular interactions of PLCL and PLLA could also be a factor, influencing the storage modulus level. Figure 2E shows the loss factor (tan δ) of the blends. Consistent with the DSC results, a single drop and a single peak appeared in the tan δ curves of PLCL90PLLA10, indicating that the blend is completely miscible. For blends with high PLLA ratios, two tan δ peaks are discernible. The tan δ_1 corresponds mainly to the PLCL amorphous phase (approximately 35 °C), whereas tan δ_2 to the PLLA amorphous phase (approximately 76 °C). Furthermore, a shift in T_g is evident, indicating that the blends at high ratios of PLLA are partially miscible. The DSC and DMA results in our study are similar to those of a previous study. Ugartemendia *et al.* discovered that PLLA/PLCL blends indicated a miscibility window below 40 wt % of the PLCL content, whereas two different phases can be assumed with two T_g values for PLLA: PLCL ratios of 20:80, 40:60, and 50:50.[36] Accordingly, it may be assumed that two phases are formed in the blends; however, the depression of T_g2 and the T_g shift suggests that PLLA and PLCL are partially miscible with good interfacial interactions between them.[43,44] Notably, the T_g values of the blends in the DMA curves are higher than those of the same sample by DSC. This may be due to the different measuring mechanisms of DMA and DSC.[45] Furthermore, the viscoelastic behavior of blends was evaluated by E' and tan δ as functions of temperature.[46] Therefore, the differences in the DMA results between the blends and PLCL demonstrate that their viscoelastic behaviors, especially their relaxation mechanisms, are changed by blending with PLLA.

2.3. Rheological Properties of PLCL/PLLA Blends.

Rheological parameters, such as complex viscosity (η^*), storage modulus (G'), loss modulus (G''), and loss tangent (tan δ), can be used to evaluate the mechanical properties and processability of the blends.[47] In this study, to investigate the effects of different mass fractions of PLLA on the rheological behaviors of PLCL/PLLA blends, frequency sweeps were performed from 0.1 to 100 rad/s at 185 °C. According to the values of T_m and T_{max} of the PLLA and PLCL/PLLA blends in the TGA test, it is rational to assume that all the polymers are in a viscous flow state during the rheological test without obvious decomposition.

Figure 3 shows the rheological properties (η^*, G', G'', and tan δ) of the blends with angular frequency (ω). As shown in Figure 3A, the η^* values of all polymers decrease with increasing ω, indicating that all the polymer melts are non-Newtonian pseudoplastic fluids and display shear-thinning (pseudo plastic) properties within the detection frequency range. Therefore, alignment, rearrangement, or disentanglement of polymer chain segments along the shear stress occurred in all the PLCL/PLLA blends, pure PLCL, and PLLA melts during the test with the increase of ω.[48] It is clear that the values of η^*, G', and G'' of PLCL are the highest in all the polymer melts, suggesting that the entanglement density of PLCL is the highest.[49] However, the G' and G'' values of PLLA are lower than that of PLCL in all frequency ranges, indicating the rigidity of PLLA is higher than that of PLCL which is inversely related to the G' and G''.[50] The values of η^*, G', and G'' of the blends decrease with the addition of PLLA. Consistent with the molecular weight of PLCL and PLLA, the η^* value of PLCL is higher than that of PLLA. The addition of PLLA widens the molecular-weight distribution of the PLCL/PLLA blends, compared with PLCL, which is helpful for the reduction of the viscosity and energy consumption of PLCL during the process. Specially, the changes caused by broadening of molecular-weight distribution are so significant that

https://doi.org/10.1021/acsomega.1c02190
ACS Omega 2021, 6, 18300−18313

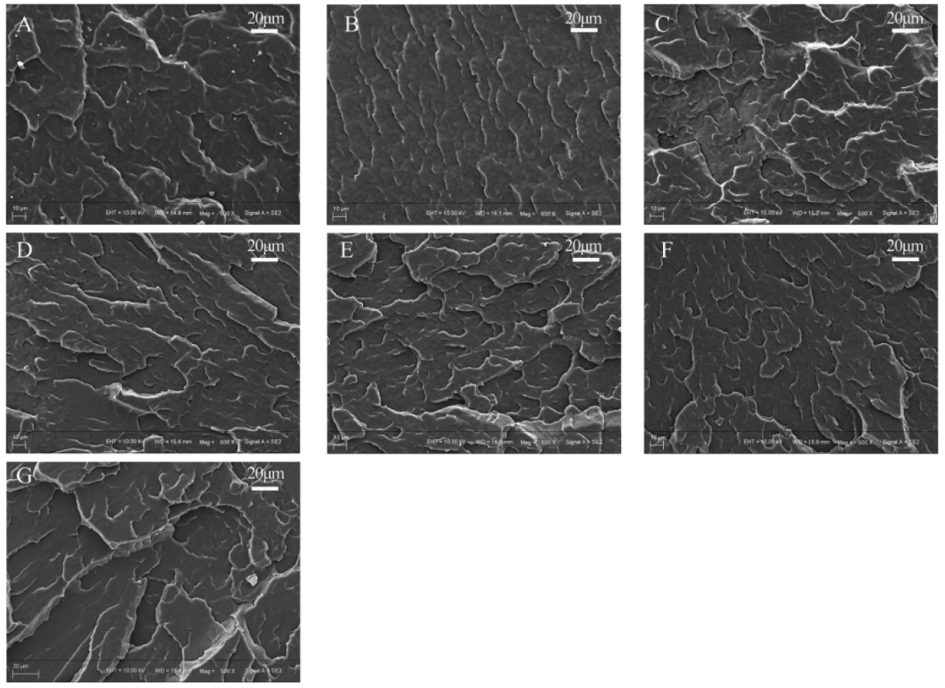

Figure 4. SEM images of the surfaces of the embrittled-broken samples. (A) PLCL; (B) PLCL90PLLA10; (C) PLCL80PLLA20; (D) PLCL70PLLA30; (E) PLCL60PLLA40; (F) PLCL50PLLA50; and (G) PLLA.

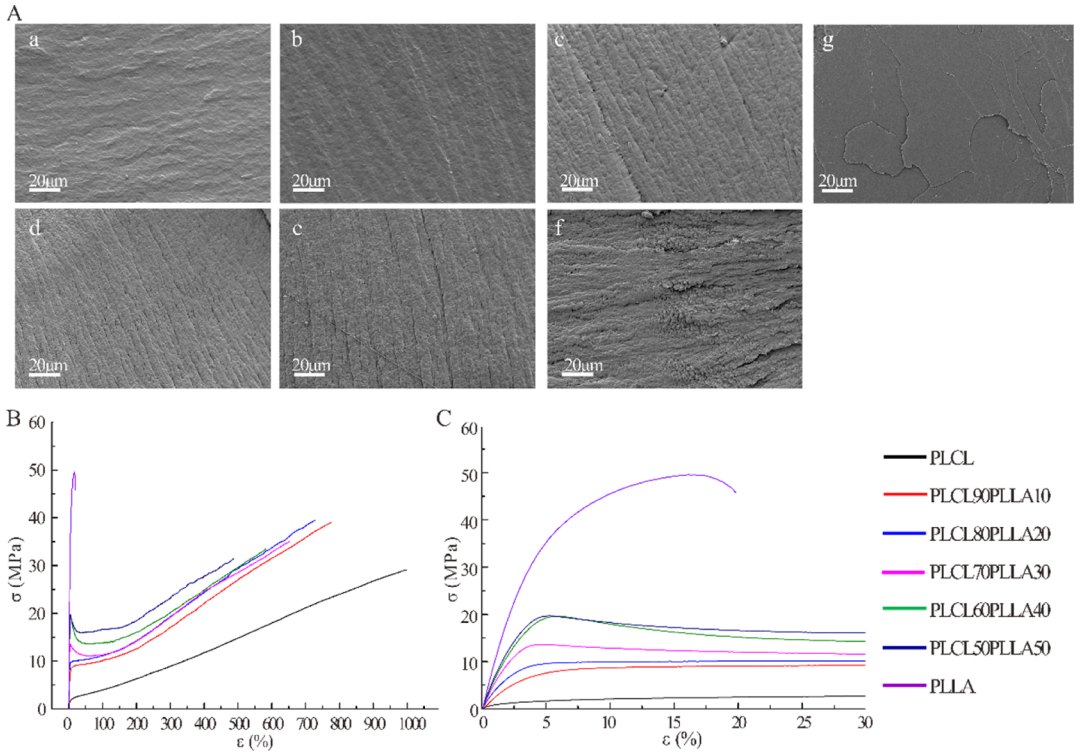

Figure 5. (A) SEM images of the tensile-fractured surfaces of PLCL/PLLA blends. (a) PLCL; (b) PLCL90PLLA10; (c) PLCL80PLLA20; (d) PLCL70PLLA30; (e) PLCL60PLLA40; (f) PLCL50PLLA50; and (g) PLLA. (B,C) Typical stress−strain curves of PLCL/PLLA blends at different mass ratios.

the η^*, G', and G'' values of PLCL/PLLA blends with 40% and 50% PLLA are even lower than those of neat PLLA. These results demonstrate that blending with PLLA improves the melt flowability of PLCL and reduces the energy consumption during the process, which is beneficial for reducing the dimensional instability caused by the extrusion swelling effect and for improving the processability of the blends.

Tan δ is calculated by G''/G' and is typically used to describe the damping characteristics of materials. As shown in Figure 3D, the tan δ value of PLCL remains at a low level in all frequency ranges, which is consistent with its high elastic

https://doi.org/10.1021/acsomega.1c02190
ACS Omega 2021, 6, 18300−18313

characteristics. However, the value of PLLA decreases from a high value at a low frequency to a low value of approximately 0 at high frequencies, indicating its good rigidity. Interestingly, unlike PLCL and PLLA, peaks appear in the curves of all the blends. These results suggest that the viscoelasticity of PLCL is altered after blending with PLLA.

2.4. Morphologies and Tensile Properties of PLCL/PLLA Blends. SEM micrographs of the cryo-fractured surfaces of the PLCL/PLLA blends are shown in Figures 4 and S1. The morphology of polymer blends is useful for determining the miscibility of the blends.[51] As shown, the surfaces of all the samples are uneven but without wire drawing, indicating that brittle fracture is happened, which is consistent with the high storage modulus (E') at low temperature in the DMA test. It can be seen that blending with PLLA appears to induce the formation of lamellar structures on the surfaces of the PLCL/PLLA blends; furthermore, no distinguishable interface but co-continuous morphologies can be observed. These results indicate that PLCL and PLLA might be miscible or at least miscible at the interface where good interfacial interactions were formed, which is consistent with the DSC and DMA results.

Next, the microstructures of the tensile-fractured surfaces of the PLCL/PLLA blends were observed *via* SEM. As shown in Figure 5A, pure PLCL shows a typical smooth fracture surface of elastomeric polymers, that is consistent with the observed deformation spontaneous recovery during the stretch-breaking test due to its high elastic recovery capacity.[8−12] On the contrary, PLLA shows a typical smooth fractured surface of brittle polymers that lacks obvious deformation during the tensile test.[36] For PLCL90PLLA10, the fracture surface is much similar to that of pure PLCL. While, for PLCL/PLLA blends with a high PLLA ratio, the fracture surfaces become rougher, and orderly arranged fiber-like structures appear and increase with the increase in PLLA. These fracture surface morphologies of the blends indicate that polymer segments are rearranged along the direction of tensile force. Therefore, plastic deformation and typical ductile fracture might occur during the tensile tests.[36] Particularly, for PLCL50PLLA50, the smooth and rough phases on the surface are clearly distinguishable, which might correspond to the PLLA and PLCL phases, respectively. This result confirms that both PLCL and PLLA show a ductile fracture behavior; however, the lengths of fiber-like structures of PLCL and PLLA are different due to their different elongation at break.[36] In addition, this result also indicates that apparent trend of phase separation appeared in PLCL50PLLA50. However, for the PLCL/PLLA blend with 10−40% PLLA, no obvious phase separation can be found from the fracture surface.

Figure 5B,C shows the representative tensile curves of neat PLCL, PLLA, and their blends at different compositions. The neat PLCL exhibits typical properties of ductile fracture with a high elongation at break and low tensile strength but without obvious yield point. The pure PLLA also displays properties of ductile fracture following a distinct yield point and a lowest elongation at break and highest tensile strength. All PLCL/PLLA blends also underwent ductile fracture but with different elongation at break and different tensile strength. Interestingly, the tensile strength of all the PLCL/PLLA blends is higher than that of PLCL, whereas the elongation at break of the blends is smaller than it. In addition, distinct yield points are observed for blends with 30−50% PLLA compared with pure PLLA. However, for PLCL90PLLA10 and PLCL80PLLA20, the yield points are much lower than that of pure PLCL. Particularly, it is discovered that the yield strengths of the blends enhanced with the increase in PLLA, especially with 30−50% PLLA. These results indicate that the addition of PLLA increases the rigidity and stiffness of PLCL.

The main tensile properties determined from these curves (Figure 5B,C), such as Young's modulus (elastic modulus), tensile strength, and elongation at break, are presented in Table 3. The elastic modulus of pure PLCL is as low as 3.66 MPa, the tensile strength is 30.41 MPa, and the elongation at break is as high as 974.47%. In contrast, the elastic modulus of pure PLLA is 877.51 MPa, the tensile strength is 47.21 MPa, and the elongation at break is only 19.7%. Compared with neat PLCL, the elastic modulus of the PLLA-blended PLCL increases significantly from 3.66 to 665.63 MPa, indicating that the addition of PLLA can increase the rigidity of PLCL, which is consistent with the results of DMA. In particular, the elastic moduli of PLCL, PLCL90PLLA10, and PLCL80PLLA20 appear similar to the modulus of native cartilage.[18,28] The PLCL/PLLA blends exhibit higher tensile strengths than the neat PLCL, whereas the elongation at break decreases from 974.47 to 509.45%. Furthermore, compared with pure PLCL, the differences in tensile strength of the blends with 10−30% PLLA are significant, whereas the elongation at break of all blends decrease significantly. Interestingly, the values of tensile strength and elongation at break for PLCL/PLLA blends with 10−40% PLLA do not differ significantly (Table S1). These is due to the different fracture behaviors of different blends, as shown in Figure 5B,C. Notably, the elastic modulus of the blend with 30% PLLA increases suddenly by more than 100 times compared with the blends with 10−20% PLLA (∼5 MPa) and the neat PLCL. Furthermore, the area below stress−strain curves was calculated to evaluate the fracture energy of blends based on Figure 5B. As shown in Figure S3, the area was not significantly different between PLCL and the blends except PLCL50PLLA50. Therefore, with the addition of PLLA, the toughness of PLCL was almost preserved, while the rigidity and stiffness of PLCL were improved.

Table 3. Tensile Properties of PLCL/PLLA Blends[a]

sample	E (MPa)	σ_{max} (MPa)	ε_u (%)
PLCL	3.66 ± 0.57	30.41 ± 2.07	974.47 ± 79.11
PLCL90PLLA10	4.69 ± 0.34	37.72 ± 1.56	753.30 ± 33.77
PLCL80PLLA20	4.98 ± 0.29	37.86 ± 1.94	719.19 ± 57.35
PLCL70PLLA30	520.79 ± 22.58	36.66 ± 2.89	688.21 ± 73.23
PLCL60PLLA40	609.92 ± 10.83	33.64 ± 4.03	642.51 ± 62.03
PLCL50PLLA50	665.63 ± 19.04	30.26 ± 3.40	509.45 ± 23.55
PLLA	877.51 ± 32.30	47.21 ± 4.93	19.70 ± 0.40

[a]Note: E, elastic modulus; σ_{max}, tensile strength; and ε_u, the ultimate strain or elongation at break.

2.5. Morphologies of 3D-Printed PLCL/PLLA Scaffolds. Figure 6 shows the 3D printing paths (Figure 6A), macrostructures (Figure 6B), and microscopic structures of the longitudinal sections (Figure 6C) of the 3D-printed scaffolds. As shown in Figure 6B, the 3D structures of all the 3D-printed scaffolds of the blends and PLCL are consistent with the designed structure, and the printed lines are continuous with no breakage. The pores of all the scaffolds of the blends are regular and evenly distributed, whereas the sizes of the pores are decreased with the increase in the filling rate. The typical

https://doi.org/10.1021/acsomega.1c02190
ACS Omega 2021, 6, 18300−18313

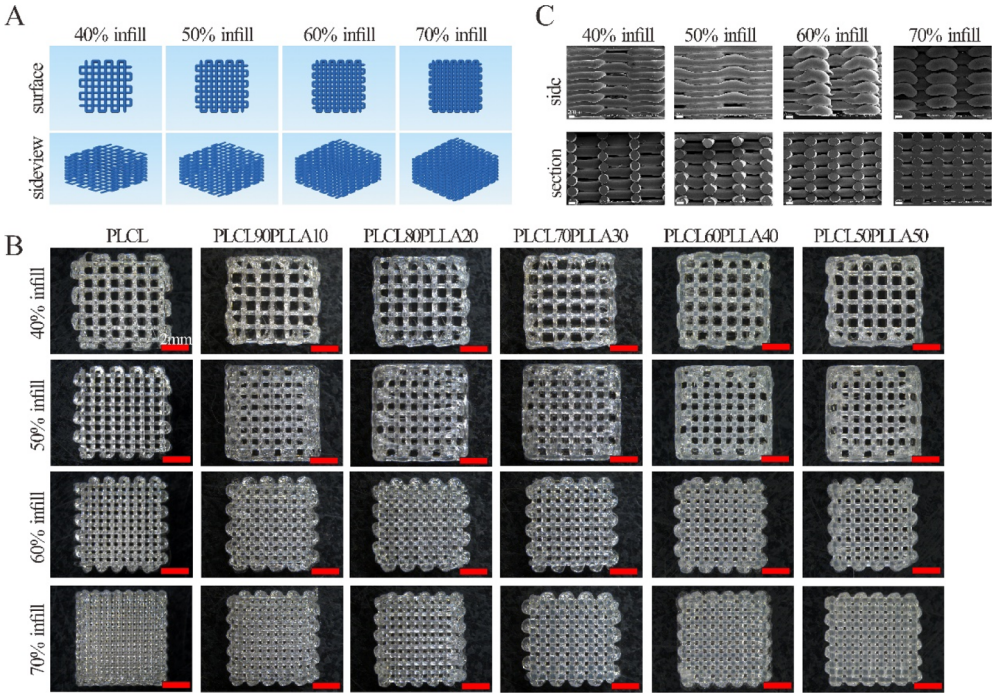

Figure 6. (A) Paths of the 3D-printing of scaffolds; (B) macroscopic structures of the scaffolds with different filling rates of PLCL/PLLA blends at different mass ratios; and (C) microscopic surface structures of the side and longitudinal section of PLCL70PLLA30 scaffolds with different filling rates.

microstructures of the edges and longitudinal sections of the PLCL/PLLA scaffolds are shown in Figure 6C. As shown, the printed lines are smooth, and the pores are uniform in size and distribute evenly and interconnectedly.

Considering that the printed structures using both PLCL and PLLA will be shrunk, owing to their viscoelastic properties induced relaxation after melt extrusion,[52] the shrinkage of the printed scaffolds was measured, and the results are shown in Table 4. Clearly, the length, width, and height of the scaffolds of all the PLCL/PLLA blends reduce, owing to the temperature change during 3D printing. These results suggest that the shrinkage ratios during the heat−cool process, such as melt-extrusion 3D printing using PLCL/PLLA blends, should be considered in the future.

2.6. Mechanical Properties of 3D-Printed Scaffolds. Furthermore, the stress relaxation behaviors of the 3D-printed scaffolds were characterized. Figure 7 shows the stress relaxation curves of the 3D-printed PLCL/PLLA scaffolds with a 70% fill rate. As shown, the stress relaxation curves of all the scaffolds are nonlinear, indicating that PLCL, PLLA, and the blends are typical viscoelastic materials.[53] All the 3D-printed scaffolds reach their maximum stresses in a short duration (approximately 30 s) at the same strain; however, their stress relaxation times ($t_{1/2}$) are different significantly. In particular, the $t_{1/2}$ of the scaffolds of the blends is shorter than that of PLCL and PLLA. In addition, it is observed that the maximum compressive stress (σ_{max}) of the blends increased with the addition of PLLA compared with PLCL.

Next, the values of elastic modulus (E), σ_{max}, and $t_{1/2}$ of all the 3D-printed scaffolds were determined, as shown in Table 5. E and σ_{max} denote important indexes of rigidity and pressure-resistant capabilities of a material. It is clear that when the scaffolds are at same filling rates, the scaffolds of PLCL shows the lowest compressive stress, whereas PLLA shows the highest. Compared with neat PLCL, the values of E and σ_{max} of the scaffolds of all PLCL/PLLA blends with the same filling rates increase significantly. The significantly increased E indicates that the rigidities of the scaffolds of the blends are effectively enhanced by the addition of PLLA compared with that of neat PLCL. The compression modulus of the PLCL/PLLA scaffolds increases from nearly 0.5 MPa to more than 30 MPa, even at lower ratios of PLLA. Furthermore, it is discovered that the values of E, σ_{max}, and $t_{1/2}$ of scaffolds of the same blends increase significantly with the increase in the filling rate during 3D printing, indicating that the mechanical properties of the 3D-printed scaffolds of the blends are adjustable by selecting suitable blending ratios of PLCL/PLLA and 3D printing parameters. It is noteworthy that the values of $t_{1/2}$ of all the scaffolds of the PLCL/PLLA blends are smaller than those of the neat PLCL, indicating that blending with PLLA can shorten the relaxation times and change the viscoelastic property of the PLCL scaffold. In this study, $t_{1/2}$ indicates the time for the stress to be relaxed to half of the initial value, which is an important parameter for characterizing the viscoelasticity of the scaffold material.[54]

2.7. Chondrocyte Growth and Gene Expression. Finally, to evaluate the potential application of the 3D-printed scaffolds in cartilage tissue engineering, the effects of three scaffolds with different mechanical properties on chondrocyte proliferation and genes expression were tested. Notably, the 70% filling rate of 3D-printed scaffolds was set up based on the findings that the scaffolds with pore size between 250 and 500 μm were better for chondrocyte proliferation and ECM production.[55] As shown in Figure 8A, it can be found that the OD values of chondrocytes on PLCL90PLLA10 and PLCL50PLLA50 scaffolds after 21 days culture are significantly higher than that of PLCL scaffold at the same 70% filling rate. This result indicates that the scaffolds of PLCL/PLLA blends are beneficial for chondrocyte growth than the PLCL scaffold. Furthermore, the mRNA expressions of chondrocyte seeding

https://doi.org/10.1021/acsomega.1c02190
ACS Omega 2021, 6, 18300−18313

Table 4. Shrinkage Ratios of the 3D-Printed Scaffolds with 70% Filling Rate

scaffolds	setting size (length × width × height) (mm)	length (mm)	shrinkage-length (%)	width (mm)	shrinkage-width (%)	height (mm)	shrinkage-height (%)
PLCL	8 × 8 × 3	6.97 ± 0.047	12.94 ± 0.59	6.62 ± 0.098	17.13 ± 1.22	2.98 ± 0.023	0.67 ± 0.77
PLCL90PLLA10	8 × 8 × 3	6.99 ± 0.063	12.66 ± 0.79	6.79 ± 0.074	15.13 ± 0.92	2.76 ± 0.013	7.92 ± 0.42
PLCL80PLLA20	8 × 8 × 3	6.88 ± 0.038	14.06 ± 0.47	6.71 ± 0.053	16.12 ± 0.66	2.79 ± 0.020	7.00 ± 0.67
PLCL70PLLA30	8 × 8 × 3	7.00 ± 0.071	12.5 ± 0.89	6.80 ± 0.082	15.06 ± 1.03	2.77 ± 0.020	7.67 ± 0.67
PLCL60PLLA40	8 × 8 × 3	6.86 ± 0.048	14.22 ± 0.60	6.64 ± 0.039	16.97 ± 0.48	2.80 ± 0.050	6.83 ± 1.67
PLCL50PLLA50	8 × 8 × 3	7.00 ± 0.074	12.56 ± 0.92	6.79 ± 0.074	15.13 ± 0.92	2.80 ± 0.000	6.67 ± 0.00

on different scaffolds are different (Figure 8B). Interestingly, although the expression of COL2A1 gene among the three groups shows no significant difference, the expression of ACAN and SOX9 of chondrocytes seeding on the PLCL90PLLA10 scaffold is significantly higher than that of the cells on PLCL50PLLA50 and PLCL scaffolds, respectively. In addition, positively stained type II collagen is observed to be evenly distributed along the 3D-printed lines in all the three kinds of scaffolds (Figure 8C), indicating that chondrocytes maintain the bioactivity to synthesize type 2 collagen after 21 days culture on the scaffolds. Taken together, these results suggest that the PLCL90PLLA10 scaffold can promote chondrocyte proliferation, increase the expressions of ACAN and SOX9, and effectively express type 2 collagen.

It is well known that the mechanical property of the scaffold plays important roles for cartilage tissue engineering and chondrogenesis. It is reported that the optimal elastic modulus for a construct for osteochondral repair is between 1 and 50 MPa *via* computational analysis.[18,56] More recently, it is found that the viscoelasticity, especially the stress relaxation of the scaffold, instead of the elasticity of the matrix is crucial in cartilage formation, repair, regeneration, and cartilage tissue engineering.[29−35] Chaudhuri *et al.* investigated the effect of stress relaxation of viscoelastic hydrogels on cartilage formation and discovered that a faster relaxation promoted cartilage matrix formation.[32] In this study, the effects of mechanical properties of the 3D-printed scaffolds on the proliferation and genes expression of chondrocyte were investigated. 3D-printed scaffolds of PLCL, PLCL90PLLA10, and PLCL50PLLA50 with 70% filling rate were selected, and they display complete different mechanical properties. Particularly, as shown in Figure 7 and Table 5, the PLCL scaffold displays the longest $t_{1/2}$, PLCL50PLLA50 with the longest $t_{1/2}$ of the blends, while PLCL90PLLA10 exhibits much shorter $t_{1/2}$. While as shown in Figure 8, compared with scaffolds of PLCL, the scaffolds of PLCL90PLLA10 and PLCL50PLLA50 can promote the growth of chondrocytes. In addition, compared with scaffolds of PLCL and PLCL50PLLA50, respectively, the PLCL90PLLA10 scaffold increases the expressions of ACAN, a gene for aggrecan, an important ECM component of chondrocyte; and SOX9, a key transcription factor for chondrogenesis.[57,58] These findings indicate that the PLCL/PLLA blend with a lower PLLA content, particularly the PLCL90PLLA10 scaffold with fast relaxation, is favorable for chondrogenesis, which is consistent with the finding of Chaudhuri *et al.*[32]

3. CONCLUSIONS

PLCL/PLLA blends are prepared using melt-extrusion methods with different mass ratios of PLLA from 10 to 50%. The blends exhibit good thermal stabilities. It is found that the miscibility of the PLCL/PLLA blends is variable; however, it is obvious that blending PLLA enhances the rigidity of PLCL and improves its melt fluidity, which result in the good printability of all PLCL/PLLA blends during the 3D printing of scaffolds. Notably, the mechanical properties of the 3D-printed scaffolds are controllable by changing the PLCL/PLLA ratios of the blends and the filling rates during 3D printing. Furthermore, blends or scaffolds with lower PLLA ratios demonstrate favorable tensile moduli, complex viscosity, compression modulus, and relaxation times for cartilage tissue engineering. In particular, the scaffolds of PLCL90PLLA10 at a 70% filling

https://doi.org/10.1021/acsomega.1c02190
ACS Omega 2021, 6, 18300−18313

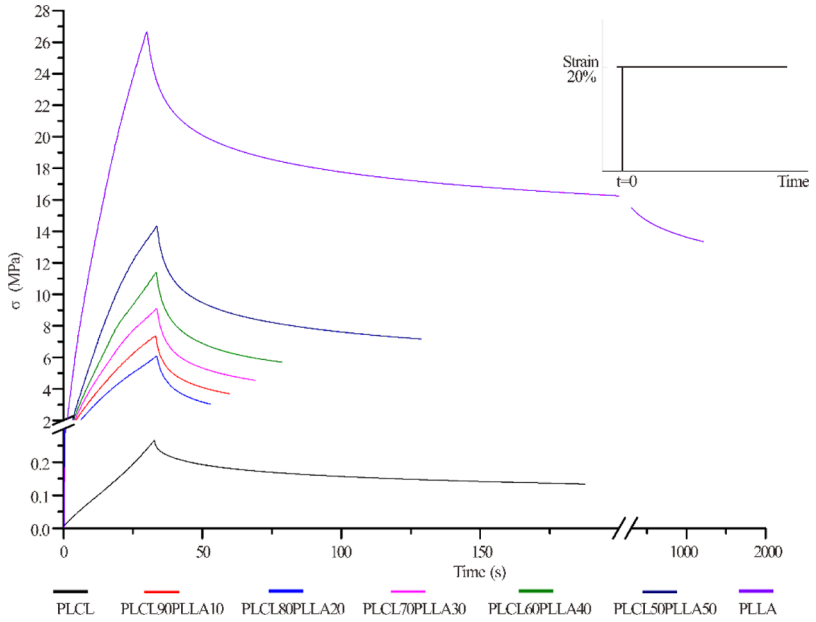

Figure 7. Stress relaxation curves of the 3D-printed scaffolds with 70% filling rate of PLCL/PLLA blends at different mass ratios.

Table 5. Mechanical Properties of the 3D-Printed Scaffolds of PLCL/PLLA Blends with Different Filling Rates[a]

scaffolds	infill ratio (%)	E (MPa)	σ_{max} (MPa)	$t_{1/2}$(s)
PLCL	40	0.52 ± 0.07	0.07 ± 0.003	110.62 ± 8.24
	50	0.76 ± 0.04	0.12 ± 0.009	155.13 ± 7.60
	60	0.96 ± 0.05	0.15 ± 0.005	177.93 ± 15.77
	70	1.60 ± 0.29	0.27 ± 0.046	170.62 ± 14.13
PLCL90PLLA10	40	34.03 ± 5.06	3.34 ± 0.53	10.36 ± 2.91
	50	42.45 ± 0.29	5.27 ± 1.40	11.12 ± 2.41
	60	54.82 ± 1.84	5.51 ± 0.88	16.00 ± 1.73
	70	62.40 ± 6.13	7.47 ± 0.56	23.32 ± 2.21
PLCL80PLLA20	40	45.45 ± 2.46	5.06 ± 0.92	17.17 ± 0.61
	50	51.88 ± 4.81	5.82 ± 0.47	17.77 ± 2.43
	60	56.74 ± 5.08	6.24 ± 0.52	19.23 ± 1.65
	70	67.89 ± 13.41	6.99 ± 1.20	19.81 ± 0.66
PLCL70PLLA30	40	42.26 ± 1.24	5.76 ± 0.69	16.64 ± 2.03
	50	56.19 ± 8.95	6.12 ± 2.00	23.97 ± 9.94
	60	63.81 ± 4.50	6.64 ± 0.49	21.27 ± 1.15
	70	72.44 ± 16.34	9.98 ± 2.27	37.64 ± 13.49
PLCL60PLLA40	40	49.37 ± 7.42	5.50 ± 2.00	20.48 ± 5.04
	50	56.73 ± 5.44	6.00 ± 1.99	32.79 ± 5.20
	60	70.58 ± 6.70	8.04 ± 0.89	36.08 ± 4.17
	70	76.97 ± 6.33	9.80 ± 1.37	40.07 ± 4.95
PLCL50PLLA50	40	53.84 ± 12.73	7.00 ± 2.16	41.32 ± 0.74
	50	67.35 ± 8.16	7.49 ± 1.39	48.94 ± 15.76
	60	81.86 ± 4.35	8.81 ± 0.12	49.48 ± 7.08
	70	97.26 ± 4.78	13.55 ± 2.52	103.77 ± 11.61
PLLA	40	68.84 ± 12.31	3.77 ± 1.31	–
	50	134.69 ± 7.70	17.87 ± 1.28	341.64 ± 10.13
	60	163.53 ± 16.89	20.22 ± 1.02	607.34 ± 66.41
	70	228.04 ± 20.41	25.27 ± 1.94	1865.61 ± 657.66

[a]Note: infill ratio, filling rate of 3D printing; E, elastic modulus; σ_{max}, compressive strength; and $t_{1/2}$, stress relaxation time.

rate with shorter $t_{1/2}$ hold great promise in cartilage tissue engineering.

4. MATERIALS AND METHODS

4.1. Materials. Both PLCL and PLLA were supplied by Jinan Daigang Biomaterial Co., Ltd. The average molecular weight of PLLA was ∼100 kDa, and the polydispersity index (D) was less than 2.0. The L-lactide/ε-caprolactone in the molar ratio of PLCL was approximately 50:50, the intrinsic viscosity was 2.9 g/dL (∼400 kDa), and the D was less than 2.0. Analytically pure dichloromethane was purchased from Tianjin Feng Chuan Chemical Reagent Technology Co., Ltd.,

https://doi.org/10.1021/acsomega.1c02190
ACS Omega 2021, 6, 18300−18313

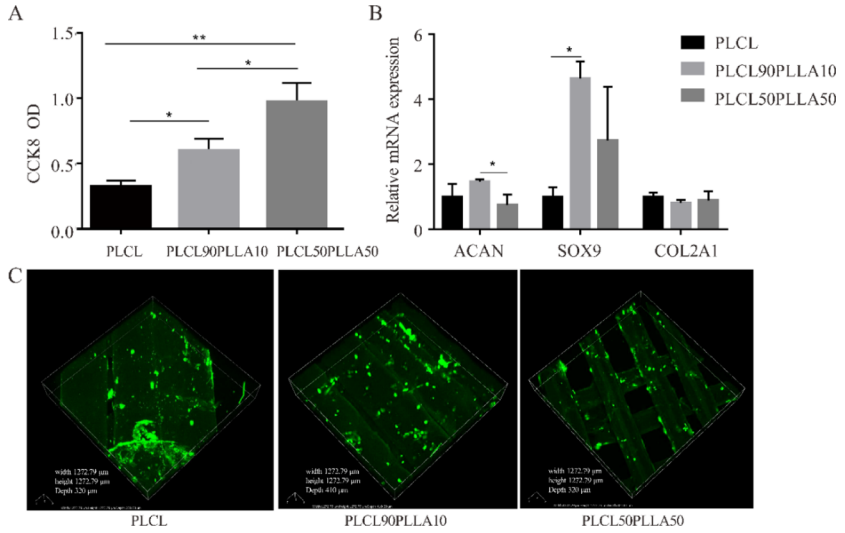

Figure 8. (A) CCK-8 assay of the chondrocytes cultured on the scaffold after 21 days of culture. $n = 4$; *$p < 0.05$, **$p < 0.01$. (B) mRNA expression levels of ACAN, SOX9, and collagen II in chondrocytes cultured on different scaffolds for 21 days. $n = 3$, *$p < 0.05$. (C) Immunofluorescence staining results of type II collagen on chondrocytes cultured on different scaffolds for 21 days.

China. Phosphate buffer (pH = 7.3−7.4) was purchased from Beijing Solarbio Science & Technology Co., Ltd, China. The cell counting kit-8 (CCK-8; CK04) was bought from Dojindo (Japan). The RNAlater (AM7020) was bought from Invitrogen (USA), and the E.Z.N.A. HP total RNA kit (R6812) was purchased from Omega Bio-tek (Canada). The GoScriptTM reverse transcription kit (A5000) and Hot Start fluorescent PCR core reagent kit (A6000) were purchased from Promega (UK). Mouse monoclonal anti-type II collagen primary antibody was purchased from Novus (USA), and FITC-labeled goat anti-mouse secondary antibody was purchased from EarthOx (USA).

4.2. Preparation of PLCL/PLLA Blends. Different mass ratios of PLCL and PLLA (Table 6) were swelled in 10 times volume of dichloromethane for 6 h, followed by stirring to obtain homogeneous mixtures. The mixed solutions were poured into Petri dishes and then placed in an electric vacuum drying oven to remove the solvent under vacuum at 80 °C for 12 h. Subsequently, the dried products were extruded through a mini-extruder (FM-12, China) of barrel length 19.72 cm, inlet diameter 11.88 mm, and outlet diameter 1.7 mm at 185 °C and 100 r/min to obtain the PLCL/PLLA blends. Finally, the blends were dried again under vacuum at 80 °C for 6 h and then used in the following experiments.

Table 6. Mass Ratios for PLCL/PLLA Blends

sample	PLCL/%	PLLA/%
PLCL	100	0
PLCL90PLLA10	90	10
PLCL80PLLA20	80	20
PLCL70PLLA30	70	30
PLCL60PLLA40	60	40
PLCL50PLLA50	50	50
PLLA	0	100

4.3. Characterization of PLCL/PLLA Blends. *4.3.1. Nuclear Magnetic Resonance Spectroscopy (^1H NMR).* The composition of the PLCL/PLLA blend was analyzed using a nuclear magnetic resonance instrument (NMR, Bruker, 400 MHz, Germany). All experiments were performed using tetramethylsilane as an internal standard and $CDCl_3$ as the solvent. The ^1H NMR spectrum was recorded with 24 repetitions and a 3 s relaxation time.

4.3.2. Thermogravimetric Analysis. TGA was performed using a thermogravimetric analyzer (Q500, TA Co., USA) based on a previously reported procedure.[59] Briefly, with a gas flow rate of 50 mL/min and under a nitrogen atmosphere, each of the vacuum-dried blends was heated from room temperature to 500 °C at a heating rate of 10 °C/min, and the temperature rise curve was recorded. Thermal kinetic analysis was performed using the software Origin. The weight of the sample was between 5 and 10 mg in all cases.

4.3.3. Differential Scanning Calorimetry. DSC studies on the blends were performed using a differential scanning calorimetry system (DSC 3^+, Mettler Toledo Co., Switzerland). The sample weight was between 5 and 10 mg in all cases. Each of the blends was tested based on a previous study.[49] Briefly, under a nitrogen atmosphere at a gas flow rate of 20 mL/min, the blend was heated from room temperature to 200 °C at a heating rate of 10 °C/min and maintained at this temperature for 5 min to eliminate the thermal history; subsequently, it was cooled to −100 °C at a cooling rate of 10 °C/min. After maintaining the samples at −100 °C for 5 min, they were reheated from −100 to 200 °C at a rate of 20 °C/min. Thermal properties were measured in the second scan, and the mid-points of the start and end of the transition in the DSC curves were used as the glass-transition (T_g) value.

4.3.4. Dynamic Thermomechanical Analysis. To perform DMA analysis, rectangular samples measuring approximately 20 mm (length) × 4 mm (width) × 0.5 mm (thickness) were prepared after hot pressing the blends into films. A DMA 242 instrument (NETZSCH Co., Germany) was operated in the tensile mode at an oscillation frequency of 3.333 Hz with a static force of 0.5 N and oscillation amplitude of 15 μm. The samples were measured over a temperature range from −120 to 150 °C at a heating rate of 3 °C/min under nitrogen gas purging.[60] Five identical specimens ($n = 5$) of each blend were tested. The measured length was 10 mm in all experiments except the catching in the clamps. The T_g values were obtained from the peaks of tan δ curves.

https://doi.org/10.1021/acsomega.1c02190
ACS Omega 2021, 6, 18300−18313

4.3.5. Rheological Properties. The dynamic rheological properties of the blends were determined using a strain-controlled rheometer (MCR 302, Anton Paar Co., Austria) equipped with parallel plates of diameter of 10 mm and a gap of approximately 0.15 mm. Frequency sweep experiments were performed at 185 °C under a nitrogen atmosphere.[41] The frequency ranged from 0.1 to 100 rad/s in an oscillatory shear at a 5% strain.

4.3.6. Morphology. To observe the morphologies of the PLCL/PLLA blends, the samples were broken by hand after embrittling them in liquid nitrogen.[60] The obtained specimens were coated with gold using a sputter coater (BAL-TEC SCD 005, Leica Co., Germany) for 5 min, and the fractured surfaces of the broken specimens were observed using a scanning electronic microscope (SUPRA 55VP Zeiss, Germany) at an acceleration voltage of 10.0 kV.

4.3.7. Tensile Behavior. Tensile tests were performed at room temperature using an electron universal testing machine (3345, Instron Co., USA). Rectangular samples were prepared, as described in the DMA test section, with n = 5. All the experiments were performed using a measurement length of 100 mm and a test speed of 10 mm/min. The elastic modulus was determined from the slope of the initial linear portion of the stress−strain curve.[61] Additionally, morphological changes of the PLCL/PLLA blends after stretch breaking were observed.[36] Briefly, samples were prepared *via* the stretching-breaking method using an Instron 3345 testing machine at a test speed of 10 mm/min. The obtained specimens were coated with gold and observed, as described above.

4.4. Three-Dimensional Printing of PLCL/PLLA Composite Scaffolds. A frame-free rectangular parallelepiped computer aided design (CAD) model measuring 8 mm × 8 mm × 3 mm (length × width × height) was designed using 123D Design 2.2.14 and saved in STL format. Subsequently, the file was imported into slicing software Simplify 3D 4.1.0, and the corresponding parameters were set as follows: layer height: 0.2 mm; filling method: straight line; filling rate: 40, 50, 60, and 70%; filling angle: 90/180°; printing temperature: 185 °C; and printing speed: 3 mm/s. The PLCL/PLLA composite scaffolds were 3D printed using a customized desktop three-axis stepper motor controlled by a single-head melt-extrusion 3D printer.

4.5. Characterization of 3D-Printed PLCL/PLLA Scaffolds. *4.5.1. Morphology.* The apparent structures of the 3D-printed scaffolds were first observed under a stereo microscope (M165 C, Leica Co., Germany). Subsequently, the scaffolds were cut along the longitudinal axis and sputter-coated with gold using a sputter coater (BAL-TEC SCD 005, Leica Co., Germany) for 5 min. Finally, the internal microscopic structures were observed using a scanning electron microscope (MERLIN Compact, Zeiss Co., Germany) at an acceleration voltage of 10.0 kV.

4.5.2. Shrinkage. Considering the shrinkage of both PLCL and PLLA after melt extrusion,[52] we measured the shrinkages of the 3D-printed PLCL/PLLA scaffolds. The length, width, and height of the printed composite scaffolds were measured using a Vernier caliper. Subsequently, the shrinkage ratios were calculated and compared with the preset parameters (n = 4 for each scaffold type).

4.5.3. Mechanical Behavior. To examine the viscoelastic properties of the blends, stress relaxation tests were performed at room temperature based on a previously reported procedure.[59] Briefly, the scaffold (n = 4 for each kind of scaffold) was characterized using an electron universal testing machine (3345, Instron Co., USA). The tests were performed based on a 20% deformation at a test speed of 1 mm/min and a load capacity of 5 kN. During the test, the same deformation was maintained up to the stress, which was reduced to half of the initial value.

4.6. *In Vitro* Chondrocyte Culture. *4.6.1. Isolation of Chondrocyte.* Japanese white rabbits were used for chondrocyte isolation. Animal experiments were performed in compliance with the guidelines made by the Animal Committee of Tianjin, China. The rabbits were allowed to acclimate to the experimental environment for at least 1 week before use. Chondrocytes were isolated using our previously reported method.[57] Briefly, rabbits (4 week old) were euthanized with an overdose of pentobarbital sodium. The cartilage was collected from the knee under aseptic conditions, washed with PBS (pH, 7.4), and then minced into small pieces (~1 mm^3). Subsequently, the cartilage pieces were digested with 0.2% type II collagenase and 0.25% pancreatin−EDTA solution for 2 h at 37 °C. The chondrocyte suspension was collected using a 70 μm nylon mesh and then washed with PBS three times. Finally, the isolated chondrocytes were cultured in high-glucose Dulbecco's modified Eagle's medium containing 10% fetal bovine serum and 1% penicillin/streptomycin. The culture medium was changed twice a week.

4.6.2. Preparation of Scaffolds for Chondrocyte Seeding. 3D-printed scaffolds of PLCL, PLCL90PLLA10, and PLCL50PLLA50 with 70% filling rate were 3D-printed and used for cell seeding. Since chondrocytes preferred the scaffolds with pore size between 250 and 500 μm for better proliferation and ECM production,[55] 3D-printed scaffolds with 70% filling rate were selected for cell seeding, of which the pore size was about 330 μm. The scaffolds were immersed into 75% alcohol solution for 4 h and then rinsed by PBS solution (pH, 7.4) three times. Subsequently, the scaffolds were placed into 48-well cell culture plates and air-dried in a clean-bench with UV radiation.

4.6.3. Chondrocyte Seeding. P2 (passage two) chondrocytes were collected following treatment with trypsin−EDTA solution and centrifugation, then were resuspended in cell culture media. Subsequently, the cells were seeded onto the 3D-printed PLCL, PLCL90PLLA10, and PLCL50PLLA50 scaffolds in the plates (n = 4). The cell concentration was 3 × 10^5 cells per scaffold with 250 μL culture medium. After overnight incubation for cell attachment, the scaffolds were transferred into new 48-well cell culture plates, adding with 250 μL/well fresh culture medium. The medium was replaced with fresh medium every 3−4 days. After 21 days culture, chondrocyte proliferation on the scaffolds was determined using CCK-8 following the manufacturer's instructions. Briefly, the scaffolds were moved into new plates with CCK-8 solution, then were incubated in the dark for 1 h. Subsequently, the scaffolds were removed, and the absorbance then was measured using a microplate reader (Thermo, Varioskan Flash, USA) at a test wavelength of 450 nm and a reference wavelength of 690 nm.

4.6.4. Gene Expression Profile of Chondrocytes. After 21 days culture as mentioned above, the mRNA expressions of COL2A1, ACAN, and SOX9 (the sequences of the primers are listed in Table S1) of the chondrocytes seeding on the scaffolds were determined using the reverse transcription-polymerase chain reaction (RT-PCR) approach. The scaffolds were moved into new plates, then total RNA was extracted using an

https://doi.org/10.1021/acsomega.1c02190
ACS Omega 2021, 6, 18300−18313

E.Z.N.A. HP total RNA kit following the manufacturer's instructions. Complementary DNA was synthesized using a GoScriptTM Reverse Transcription reagent kit, as described by the manufacturer. RT-PCR was performed using a Hot Start fluorescent PCR core reagent kit, according to the manufacturer's instructions on an ABI PRISM 7500 real-time PCR system (Applied Biosystems, Foster, CA, USA). Finally, the mRNA expressions were determined using the $2^{-\Delta\Delta CT}$ method using glyceraldehyde-3-phosphate dehydrogenase (GAPDH) as the reference gene.

4.6.5. Immunofluorescence Staining. Furthermore, the expression of the type II collagen of chondrocytes seeding on the scaffolds after 21 days culture as mentioned above was assessed using immunofluorescence staining. The scaffolds were fixed with 4% paraformaldehyde and then were sectioned manually at a thickness of about 500 μm. After washing with PBS three times (5 min each time), the sections were permeabilized with 0.01% Triton X-100 for 10 min followed by PBS rinsing. Subsequently, the sections were blocked by 5% bovine serum albumin for 30 min, incubated with anti-type II collagen primary antibody (1:100) overnight at 4 °C, and followed by incubation with FITC-labeled secondary antibody (1:100) for 1 h at 37 °C in the dark. Finally, washing twice with PBS (2 min each time), the stained sections were mounted onto glass slides with 50% glycerol. The slides were put on a confocal laser scanning microscope (Nikon Eclipse Ti, Japan). 3D images were scanned along with longitudinal gel depth from base surface (Z) with Z axial interval of 10 μm. The signal intensities of fluorescence for the immunofluorescence-stained type II collagen were obtained by excitation at the wavelengths of 488 nm.

4.7. Statistical Analysis. All data were expressed as mean ± standard deviation (SD). The statistical significance of differences between groups was analyzed using either a *t*-test or a one-way analysis of variance. All statistical analyses were performed using SPSS (version 19) software based on statistically independent observations, and differences were considered to be statistically significant when the *P*-value was less than 0.05.

■ ASSOCIATED CONTENT

Supporting Information

The Supporting Information is available free of charge at https://pubs.acs.org/doi/10.1021/acsomega.1c02190.

SEM images of the surfaces of the embrittled-broken samples; difference in tensile properties of PLCL/PLLA blends; X-ray diffraction patterns of the filaments of PLCL/PLLA blends; area below stress−strain curves of PLCL/PLLA blends at different mass ratios; and mechanical properties of the 3D-printed scaffolds of PLCL/PLLA blends with different filling rates (PDF)

■ AUTHOR INFORMATION

Corresponding Authors

Xuemin Li − *The Key Laboratory of Biomedical Material of Tianjin, Biomedical Barriers Research Center, Chinese Academy of Medical Sciences & Peking Union Medical College Institute of Biomedical Engineering, Tianjin 300192, P.R. China;* orcid.org/0000-0001-7702-4826; Email: lixuemin-7205@vip.sina.com

Qiqing Zhang − *The Key Laboratory of Biomedical Material of Tianjin, Biomedical Barriers Research Center, Chinese Academy of Medical Sciences & Peking Union Medical College Institute of Biomedical Engineering, Tianjin 300192, P.R. China; Institute of Biomedical Engineering, the Second Clinical Medical College, Jinan University (Shenzhen People's Hospital), Shenzhen 518020 Guangdong, P.R. China;* Email: zhangqiq@126.com

Authors

Ruiping Duan − *The Key Laboratory of Biomedical Material of Tianjin, Biomedical Barriers Research Center, Chinese Academy of Medical Sciences & Peking Union Medical College Institute of Biomedical Engineering, Tianjin 300192, P.R. China;* orcid.org/0000-0001-9114-2837

Yimeng Wang − *The Key Laboratory of Biomedical Material of Tianjin, Biomedical Barriers Research Center, Chinese Academy of Medical Sciences & Peking Union Medical College Institute of Biomedical Engineering, Tianjin 300192, P.R. China*

Yiyun Zhang − *The Key Laboratory of Biomedical Material of Tianjin, Biomedical Barriers Research Center, Chinese Academy of Medical Sciences & Peking Union Medical College Institute of Biomedical Engineering, Tianjin 300192, P.R. China*

Ziqiang Wang − *The Key Laboratory of Biomedical Material of Tianjin, Biomedical Barriers Research Center, Chinese Academy of Medical Sciences & Peking Union Medical College Institute of Biomedical Engineering, Tianjin 300192, P.R. China*

Fuchong Du − *The Key Laboratory of Biomedical Material of Tianjin, Biomedical Barriers Research Center, Chinese Academy of Medical Sciences & Peking Union Medical College Institute of Biomedical Engineering, Tianjin 300192, P.R. China*

Bo Du − *The Key Laboratory of Biomedical Material of Tianjin, Biomedical Barriers Research Center, Chinese Academy of Medical Sciences & Peking Union Medical College Institute of Biomedical Engineering, Tianjin 300192, P.R. China*

Danning Su − *The Key Laboratory of Biomedical Material of Tianjin, Biomedical Barriers Research Center, Chinese Academy of Medical Sciences & Peking Union Medical College Institute of Biomedical Engineering, Tianjin 300192, P.R. China*

Lingrong Liu − *The Key Laboratory of Biomedical Material of Tianjin, Biomedical Barriers Research Center, Chinese Academy of Medical Sciences & Peking Union Medical College Institute of Biomedical Engineering, Tianjin 300192, P.R. China;* orcid.org/0000-0001-9152-7737

Complete contact information is available at: https://pubs.acs.org/10.1021/acsomega.1c02190

Author Contributions

R. D., Y. W., Y. Z., and Z. W. contributed equally. The manuscript was written through contributions of all authors. All authors have given approval to the final version of the manuscript.

Notes

The authors declare no competing financial interest.

■ ACKNOWLEDGMENTS

This work was supported by the National Natural Science Foundation of China (81972043 and 81501578), the CAMS

Innovation Fund for Medical Sciences (CAMS-2017-I2M-1-007), the Fundamental Research Funds for the Central Universities (3332019102), and the Key Project of Guang-Dong Basic and Applied Basic Research Foundation (2020B1515120091).

REFERENCES

(1) Richbourg, N. R.; Peppas, N. A.; Sikavitsas, V. I. Tuning the biomimetic behavior of scaffolds for regenerative medicine through surface modifications. *J. Regen. Med. Tissue Eng.* **2019**, *13*, 1275−1293.
(2) Murphy, S. V.; Atala, A. 3D bioprinting of tissues and organs. *Nat. Biotechnol.* **2014**, *32*, 773−785.
(3) Zhang, Y. S.; Yue, K.; Aleman, J.; Mollazadeh-Moghaddam, K.; Bakht, S. M.; Yang, J.; Jia, W.; Dell'Erba, V.; Assawes, P.; Shin, S. R.; Dokmeci, M. R.; Oklu, R.; Khademhosseini, A. 3D Bioprinting for Tissue and Organ Fabrication. *Ann. Biomed. Eng.* **2017**, *45*, 148−163.
(4) Mandrycky, C.; Wang, Z.; Kim, K.; Kim, D.-H. 3D Bioprinting for Engineering Complex Tissues. *Biotechnol. Adv.* **2016**, *34*, 422−434.
(5) Liu, W.; Feng, Z.; Ou-Yang, W.; Pan, X.; Wang, X.; Huang, P.; Zhang, C.; Kong, D.; Wang, W. 3D Printing of Implantable Elastic PLCL Copolymer Scaffolds. *Soft Matter* **2020**, *16*, 2141−2148.
(6) Kelnar, I.; Kratochvíl, J.; Kaprálková, L.; Zhigunov, A.; Nevoralová, M. Graphite nanoplatelets-modified PLA/PCL: Effect of blend ratio and nanofiller localization on structure and properties. *J. Mech. Behav. Biomed. Mater.* **2017**, *71*, 271−278.
(7) He, Y.; Liu, W.; Guan, L.; Chen, J.; Duan, L.; Jia, Z.; Huang, J.; Li, W.; Liu, J.; Xiong, J.; Liu, L.; Wang, D. 3D-Printed PLCL Scaffold Coated with Collagen Type I and Its Biocompatibility. *BioMed Res. Int.* **2018**, *2018*, 5147156.
(8) Yoo, J.; Park, J. H.; Kwon, Y. W.; Chung, J. J.; Choi, I. C.; Nam, J. J.; Lee, H. S.; Jeon, E. Y.; Lee, K.; Kim, S. H.; Jung, Y.; Park, J. W. Augmented peripheral nerve regeneration through elastic nerve guidance conduits prepared using a porous PLCL membrane with a 3D printed collagen hydrogel. *Biomater. Sci.* **2020**, *8*, 6261−6271.
(9) Jeong, S. I.; Kim, S. H.; Kim, Y. H.; Jung, Y.; Kwon, J. H.; Kim, B.-S.; Lee, Y. M. Manufacture of elastic biodegradable PLCL scaffolds for mechano-active vascular tissue engineering. *J. Biomater. Sci. Polym. Ed.* **2004**, *15*, 645−660.
(10) Jeong, S. I.; Kwon, J. H.; Lim, J. I.; Cho, S.-W.; Jung, Y.; Sung, W. J.; Kim, S. H.; Kim, Y. H.; Lee, Y. M.; Kim, B.-S.; Choi, C. Y.; Kim, S.-J. Mechano-active tissue engineering of vascular smooth muscle using pulsatile perfusion bioreactors and elastic PLCL scaffolds. *Biomaterials* **2005**, *26*, 1405−1411.
(11) Akkouch, A.; Zhang, Z.; Rouabhia, M. Engineering bone tissue using human dental pulp stem cells and an osteogenic collagen-hydroxyapatite-poly (L-lactide-co-ε-caprolactone) scaffold. *J. Appl. Biomater.* **2014**, *28*, 922−936.
(12) Wang, W.; Hu, J.; He, C.; Nie, W.; Feng, W.; Qiu, K.; Zhou, X.; Gao, Y.; Wang, G. Heparinized PLLA/PLCL nanofibrous scaffold for potential engineering of small-diameter blood vessel: Tunable elasticity and anticoagulation property. *J. Biomed. Mater. Res., Part A* **2014**, *103*, 1784−1797.
(13) Kim, M.; Hong, B.; Lee, J.; Kim, S. E.; Kang, S. S.; Kim, Y. H.; Tae, G. Composite System of PLCL Scaffold and Heparin-Based Hydrogel for Regeneration of Partial-Thickness Cartilage Defects. *Biomacromolecules* **2012**, *13*, 2287−2298.
(14) Xie, J.; Ihara, M.; Jung, Y.; Kwon, I. K.; Kim, S. H.; Kim, Y. H.; Matsuda, T. Mechano-active Scaffold Design Based on Microporous poly(L-lactide-co-epsilon-caprolactone) for Articular Cartilage Tissue Engineering: Dependence of Porosity on Compression Force-Applied Mechanical Behaviors. *Tissue Eng.* **2006**, *12*, 449−458.
(15) Xie, J.; Han, Z.; Naito, M.; Maeyama, A.; Kim, S. H.; Kim, Y. H.; Matsuda, T. Articular Cartilage Tissue Engineering Based on a Mechano-Active Scaffold Made of poly(L-lactide-co-epsilon-caprolactone): In Vivo Performance in Adult Rabbits. *J. Biomed. Mater. Res. B Appl. Biomater.* **2010**, *94*, 80−88.
(16) Kim, S. H.; Jung, Y.; Kim, S. H. A Biocompatible Tissue Scaffold Produced by Supercritical Fluid Processing for Cartilage Tissue Engineering. *Tissue Eng., Part C* **2013**, *19*, 181−188.
(17) Jung, Y.; Kim, S. H.; You, H. J.; Kim, S.-H.; Ha Kim, Y.; Min, B. G. Application of an Elastic Biodegradable poly(L-lactide-co-epsilon-caprolactone) Scaffold for Cartilage Tissue Regeneration. *J. Biomater. Sci. Polym. Ed.* **2008**, *19*, 1073−1085.
(18) Barron, V.; Neary, M.; Mohamed, K. M. S.; Ansboro, S.; Shaw, G.; O'Malley, G.; Rooney, N.; Barry, F.; Murphy, M. Evaluation of the Early *In Vivo* Response of a Functionally Graded Macroporous Scaffold in an Osteochondral Defect in a Rabbit Model. *Ann. Biomed. Eng.* **2016**, *44*, 1832−1844.
(19) Jung, Y.; Park, M. S.; Lee, J. W.; Kim, Y. H.; Kim, S.-H.; Kim, S. H. Cartilage Regeneration With Highly-Elastic Three-Dimensional Scaffolds Prepared From Biodegradable poly(L-lactide-co-epsilon-caprolactone). *Biomaterials* **2008**, *29*, 4630−4636.
(20) He, X.; Fu, W.; Feng, B.; Wang, H.; Liu, Z.; Yin, M.; Wang, W.; Zheng, J. Electrospun collagen-poly(L-lactic acid-co-ε-caprolactone) membranes for cartilage tissue engineering. *Regen. Med.* **2013**, *8*, 425−436.
(21) Jin, G.-Z.; Kim, J.-J.; Park, J.-H.; Seo, S.-J.; Kim, J.-H.; Lee, E.-J.; Kim, H.-W. Biphasic Nanofibrous Constructs With Seeded Cell Layers for Osteochondral Repair. *Tissue Eng., Part C* **2014**, *20*, 895−904.
(22) Lee, S.; Lee, K.; Kim, S.; Jung, Y. Enhanced Cartilaginous Tissue Formation With a Cell Aggregate-Fibrin-Polymer Scaffold Complex. *Polymers* **2017**, *9*, 348.
(23) Yang, Z.; Wu, Y.; Li, C.; Zhang, T.; Zou, Y.; Hui, J. H. P.; Ge, Z.; Lee, E. H. Improved Mesenchymal Stem Cells Attachment and in Vitro Cartilage Tissue Formation on Chitosan-Modified poly(L-lactide-co-epsilon-caprolactone) Scaffold. *Tissue Eng., Part A* **2012**, *18*, 242−251.
(24) Jung, Y.; Kim, S.-H.; Kim, Y. H.; Kim, S. H. The Effect of Hybridization of Hydrogels and poly(L-lactide-co-epsilon-caprolactone) Scaffolds on Cartilage Tissue Engineering. *J. Biomater. Sci. Polym. Ed.* **2010**, *21*, 581−592.
(25) Li, C.; Zhang, J.; Li, Y.; Moran, S.; Khang, G.; Ge, Z. Poly (L-Lactide-Co-Caprolactone) Scaffolds Enhanced With Poly (β-Hydroxybutyrate-Co-β-Hydroxyvalerate) Microspheres for Cartilage Regeneration. *Biomed. Mater.* **2013**, *8*, 025005.
(26) Kim, S. H.; Kim, S. H.; Jung, Y. TGF-β3 encapsulated PLCL scaffold by a supercritical CO2-HFIP co-solvent system for cartilage tissue engineering. *J. Controlled Release* **2015**, *206*, 101−107.
(27) Guo, T.; Noshin, M.; Baker, H. B.; Taskoy, E.; Meredith, S. J.; Tang, Q.; Ringel, J. P.; Lerman, M. J.; Chen, Y.; Packer, J. D.; Fisher, J. P. 3D Printed Biofunctionalized Scaffolds for Microfracture Repair of Cartilage Defects. *Biomaterials* **2018**, *185*, 219−231.
(28) Li, C.; Wang, L.; Yang, Z.; Kim, G.; Chen, H.; Ge, Z. A Viscoelastic Chitosan- Modified Three-Dimensional Porous poly(L-lactide-co-ε-caprolactone) Scaffold for Cartilage Tissue Engineering. *J. Biomater. Sci. Polym. Ed.* **2012**, *23*, 405−424.
(29) Huang, D.; Huang, Y.; Xiao, Y.; Yang, X.; Lin, H.; Feng, G.; Zhu, X.; Zhang, X. Viscoelasticity in natural tissues and engineered scaffolds for tissue reconstruction. *Acta Biomater.* **2019**, *97*, 74−92.
(30) Lawless, B. M.; Sadeghi, H.; Temple, D. K.; Dhaliwal, H.; Espino, D. M.; Hukins, D. W. L. Viscoelasticity of articular cartilage: analysing the effect of induced stress and the restraint of bone in a dynamic environment. *J. Mech. Behav. Biomed. Mater.* **2017**, *75*, 293−301.
(31) Seidenstuecker, M.; Watrinet, J.; Bernstein, A.; Suedkamp, N. P.; Latorre, S. H.; Maks, A.; Mayr, H. O. Viscoelasticity and histology of the human cartilage in healthy and degenerated conditions of the knee. *J. Orthop. Surg. Res.* **2019**, *14*, 256.
(32) Lee, H.-p.; Gu, L.; Mooney, D. J.; Levenston, M. E.; Chaudhuri, O. Mechanical confinement regulates cartilage matrix formation by chondrocytes. *Nat. Mater.* **2017**, *16*, 1243−1251.
(33) Lin, D.; Cai, B.; Wang, L.; Cai, L.; Wang, Z.; Xie, J.; Lv, Q.-x.; Yuan, Y.; Liu, C.; Shen, S. G. A Viscoelastic PEGylated Poly(glycerol

https://doi.org/10.1021/acsomega.1c02190
ACS Omega 2021, 6, 18300−18313

Sebacate)-Based Bilayer Scaffold for Cartilage Regeneration in Full-Thickness Osteochondral Defect. *Biomaterials* **2020**, *253*, 120095.
(34) Chaudhuri, O.; Gu, L.; Klumpers, D.; Darnell, M.; Bencherif, S. A.; Weaver, J. C.; Huebsch, N.; Lee, H.-p.; Lippens, E.; Duda, G. N.; Mooney, D. J. Hydrogels With Tunable Stress Relaxation Regulate Stem Cell Fate and Activity. *Nat. Mater.* **2016**, *15*, 326−334.
(35) Chaudhuri, O.; Gu, L.; Darnell, M.; Klumpers, D.; Bencherif, S. A.; Weaver, J. C.; Huebsch, N.; Mooney, D. J. Substrate stress relaxation regulates cell spreading. *Nat. Commun.* **2015**, *6*, 6365.
(36) Ugartemendia, J. M.; Larrañaga, A.; Amestoy, H.; Etxeberria, A.; Sarasua, J. R. Tougher biodegradable polylactide system for bone fracture fixations: Miscibility study, phase morphology and mechanical properties. *Eur. Polym. J.* **2018**, *98*, 411−419.
(37) Zhang, K.; Fu, Q.; Yoo, J.; Chen, X.; Chandra, P.; Mo, X.; Song, L.; Atala, A.; Zhao, W. 3D Bioprinting of Urethra With PCL/PLCL Blend and Dual Autologous Cells in Fibrin Hydrogel: An in Vitro Evaluation of Biomimetic Mechanical Property and Cell Growth Environment. *Acta Biomater.* **2017**, *50*, 154−164.
(38) Garkhal, K.; Verma, S.; Jonnalagadda, S.; Kumar, N. Fast degradable poly(L-lactide-co-ε-caprolactone) microspheres for tissue engineering: Synthesis, characterization, and degradation behavior. *J. Polym. Sci., Part A: Polym. Chem.* **2007**, *45*, 2755−2764.
(39) Signori, F.; Coltelli, M.-B.; Bronco, S. Thermal degradation of poly(lactic acid) (PLA) and poly(butylene adipate-co-terephthalate) (PBAT) and their blends upon melt processing. *Polym. Degrad. Stabil.* **2009**, *94*, 74−82.
(40) Zong, R.; Hu, Y.; Liu, N.; Wang, S.; Liao, G. Evaluation of the thermal degradation of PC/ABS/montmorillonite nanocomposites. *Polym. Adv. Technol.* **2005**, *16*, 725−731.
(41) Li, Y.; Shimizu, H. Improvement in toughness of poly(l-lactide) (PLLA) through reactive blending with acrylonitrile-butadiene-styrene copolymer (ABS): Morphology and properties. *Eur. Polym. J.* **2009**, *45*, 738−746.
(42) Ostafinska, A.; Fortelný, I.; Hodan, J.; Krejčíková, S.; Nevoralová, M.; Kredatusová, J.; Kruliš, Z.; Kotek, J.; Šlouf, M. Strong synergistic effects in PLA/PCL blends: Impact of PLA matrix viscosity. *J. Mech. Behav. Biomed. Mater.* **2017**, *69*, 229−241.
(43) Zhao, Q.; Ding, Y.; Yang, B.; Ning, N.; Fu, Q. Highly efficient toughening effect of ultrafine full-vulcanized powdered rubber on poly(lactic acid) (PLA). *Polym. Test.* **2013**, *32*, 299−305.
(44) Mofokeng, J. P.; Luyt, A. S. Dynamic mechanical properties of PLA/PHBV, PLA/PCL, PHBV/PCL blends and their nanocomposites with TiO_2 as nanofiller. *Thermochim. Acta* **2015**, *613*, 41−53.
(45) Hatakeyama, T. *Thermal Analysis: Fundamentals and Applications to Polymer Science*; John Wiley & Sons: New York, 1994.
(46) Bernardes, G. P.; Rosa Luiz, N.; Santana, R. M. C.; Camargo Forte, M. M. Influence of the morphology and viscoelasticity on the thermomechanical properties of poly(lactic acid)/thermoplastic polyurethane blends compatibilized with ethylene-ester copolymer. *J. Appl. Polym. Sci.* **2020**, *137*, 48926.
(47) Shi, Y.-D.; Zhang, K.; Chen, Y.-F.; Zeng, J.-B.; Wang, M. New approach to morphological control for polypropylene/polyethylene blends via magnetic self-organization. *Mater. Des.* **2017**, *117*, 24−36.
(48) Sinthavathavorn, W.; Nithitanakul, M.; Grady, B. P.; Magaraphan, R. Melt rheology and die swell of PA6/LDPE blends by using lithium ionomer as a compatibilizer. *Polym. Bull.* **2009**, *63*, 23−35.
(49) Shi, Y.-D.; Cheng, Y.-H.; Chen, Y.-F.; Zhang, K.; Zeng, J.-B.; Wang, M. Morphology, rheological and crystallization behavior in thermoplastic polyurethane toughed poly(L-lactide) with stereocomplex crystallites. *Polym. Test.* **2017**, *62*, 1−12.
(50) Vadillo, D. C.; Tuladhar, T. R.; Mulji, A. C.; Mackley, M. R. The rheological characterization of linear viscoelasticity for ink jet fluids using piezo axial vibrator and torsion resonator rheometers. *J. Rheol.* **2010**, *54*, 781−795.
(51) Wang, N.; Yu, J.; Ma, X. Preparation and characterization of thermoplastic starch/PLA blends by one-step reactive extrusion. *Polym. Int.* **2007**, *56*, 1440−1447.
(52) Arhaliass, A.; Bouvier, J. M.; Legrand, J. Melt growth and shrinkage at the exit of the die in the extrusion-cooking process. *J. Food Eng.* **2003**, *60*, 185−192.
(53) Schiavi, A.; Prato, A. Evidences of non-linear short-term stress relaxation in polymers. *Polym. Test.* **2017**, *59*, 220−229.
(54) Liang, X.; Gao, J.; Xu, W.; Wang, X.; Shen, Y.; Tang, J.; Cui, S.; Yang, X.; Liu, Q.; Yu, L.; Ding, J. Structural mechanics of 3D-printed poly(lactic acid) scaffolds with tetragonal, hexagonal and wheel-like designs. *Biofabrication* **2019**, *11*, 035009.
(55) Lien, S.-M.; Ko, L.-Y.; Huang, T.-J. Effect of pore size on ECM Secretion and cell growth in gelatin scaffold for articular cartilage tissue engineering. *Acta Biomater.* **2009**, *5*, 670−679.
(56) Kelly, D. J.; Prendergast, P. J. Prediction of the optimal mechanical properties for a scaffold used in osteochondral defect repair. *Tissue Eng.* **2006**, *12*, 2509−2519.
(57) Yang, W.; Cao, Y.; Zhang, Z.; Du, F.; Shi, Y.; Li, X.; Zhang, Q. Targeted delivery of FGF2 to subchondral bone enhanced the repair of articular cartilage defect. *Acta Biomater.* **2018**, *69*, 170−182.
(58) Antunes, B. P.; Vainieri, M. L.; Alini, M.; Monsonego-Ornan, E.; Grad, S.; Yayon, A. Enhanced chondrogenic phenotype of primary bovine articular chondrocytes in Fibrin-Hyaluronan hydrogel by multi-axial mechanical loading and FGF18. *Acta Biomater.* **2020**, *105*, 170−179.
(59) Revati, R.; Abdul Majid, M. S.; Ridzuan, M. J. M.; Normahira, M.; Mohd Nasir, N. F.; Rahman, M. N. Y.; Gibson, A. G. Mechanical, thermal and morphological characterisation of 3D porous Pennisetum purpureum/PLA biocomposites scaffold. *Mater. Sci. Eng. C* **2017**, *75*, 752−759.
(60) Zuo, D.-Y.; Zhang, L.; Yi, C.-H.; Zuo, H.-T. Effects of compatibility of poly(L-lactic-acid) and thermoplastic polyurethane on mechanical property of blend fiber. *Polym. Adv. Technol.* **2014**, *25*, 1406−1411.
(61) Gupta, B.; Geeta, A.; Ray, A. R. Preparation of poly(ε-caprolactone)/poly(ε-caprolactone-co-lactide) (PCL/PLCL) blend filament by melt spinning. *J. Appl. Polym. Sci.* **2011**, *123*, 1944−1950.

https://doi.org/10.1021/acsomega.1c02190
ACS Omega 2021, 6, 18300−18313